The Dynamical Placement of Mega-Constellations

Nathan Reiland[1], Aaron J Rosengren[1], Davide Amato[1], Claudio Bombardelli[2]

1) The University of Arizona, Tucson, AZ, United States

2) The Technical University of Madrid, Madrid, Spain

CODER 2018 Workshop on Orbital Debris Education and Research

College Park, Maryland, November 13th-15th 2018

Outline

Background information

Goals of the study

Phase-space cartography

- Overview of methods
- Implementation
- Results

Estimation of collision probability

- Background theory
- Implementation
- Results

Summary of key findings

Conclusions

Outline

Background information

Goals of the study

Phase-space cartography

- Overview of methods
- Implementation
- Results

Estimation of collision probability

- Background theory
- Implementation
- Results

Summary of key findings

Conclusions

The current state of affairs

THE UNIVERSITY OF ARIZONA

There are currently $\sim$17,000 entries in the NORAD catalogue of tracked objects.

The current state of affairs

THE UNIVERSITY OF ARIZONA

There are currently $\sim$17,000 entries in the NORAD catalogue of tracked objects.

13217 LEO objects
2620 MEO objects
Only $\sim$1,700 of these objects are active satellites

The future of near-Earth space

In the coming years, satellite mega-constellations will be the driving force behind the growth of objects in near-Earth space.

The future of near-Earth space

THE UNIVERSITY OF ARIZONA

In the coming years, satellite mega-constellations will be the driving force behind the growth of objects in near-Earth space.

Currently Proposed Constellations:

OneWeb LEO: 1980 sats ($h = 1200$ km)
OneWeb MEO: 2560 sats ($h = 8500$ km)
SpaceX (*Starlink*): 4425 sats ($h = 1150$ km)
Boeing V-Band: 2956 sats ($h = 1000$ km)
Further proposals: Theia (120 sats), MULTUS (140 sats), ...

The future of near-Earth space

THE UNIVERSITY OF ARIZONA

OneWeb LEO

	Nominal	Interval
Total satellites	1980	—
Number of planes	36	–
Satellites per plane	55	—
Altitude	1200 km	–
i	87.9°	–
Ω	0°	0° – 178.5°

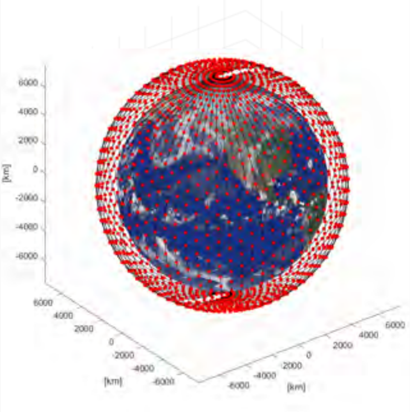

The future of near-Earth space

OneWeb MEO

	Nominal	Interval
Total satellites	2560	—
Number of planes	32	–
Satellites per plane	80	—
Altitude	8500 km	±200 km
i	45°	±2°
Ω	0°	0° – 326.25°

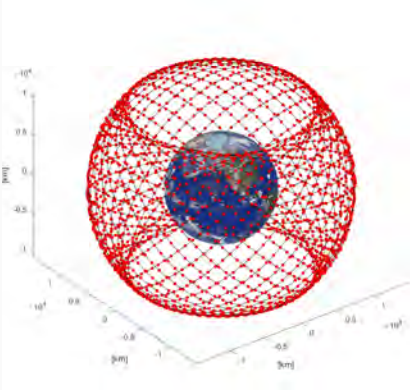

The future of near-Earth space

Future LEO catalogue:

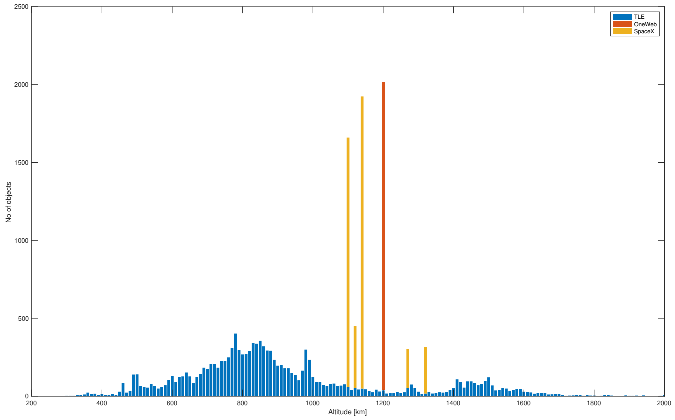

The future of near-Earth space

Future MEO catalogue:

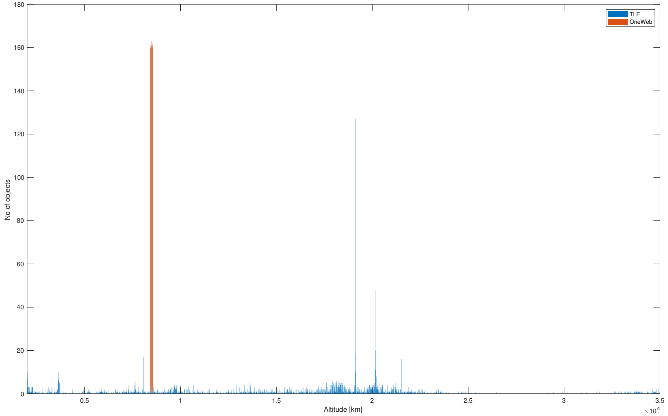

Goals of the Study

1. Study the dynamical stability of OneWeb LEO and MEO.
2. Predict the average collision probability of OneWeb LEO.

Phase-space cartography

Background information

Goals of the study

Phase-space cartography

- Overview of methods
- Implementation
- Results

Estimation of collision probability

- Background theory
- Implementation
- Results

Summary of key findings

Conclusions

Phase-space cartography

The location and amplitude of lunisolar and SRP resonances in the near-Earth phase space determine orbital stability and lifetime.

Analytical studies relying on the analysis of the perturbing function can be used to generate resonance webs.

Phase-space cartography

Lunar semi-secular resonances

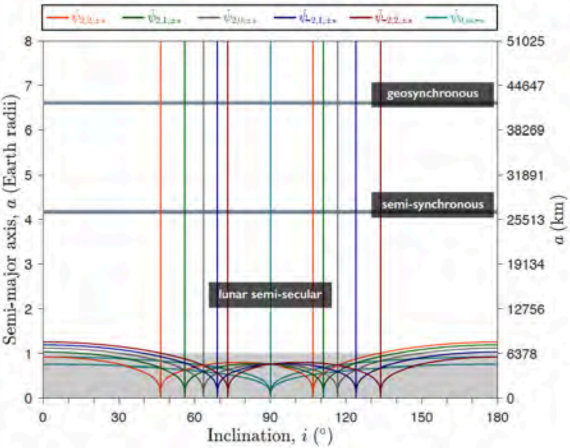

The oblateness *apsidal* and *nodal* precession overshadows the lunisolar effects

$$\dot{\omega} \approx 4.98 (R/a)^{\frac{7}{2}} \frac{5\cos^2 I - 1)}{(1-e^2)^2}\,{}^\circ/\mathrm{d}$$

$$\dot{\Omega} \approx -9.97 (R/a)^{\frac{7}{2}} \frac{\cos I}{(1-e^2)^2}\,{}^\circ/\mathrm{d}$$

$$\dot{\Omega}_{\mathrm{M}} \approx -0.053^\circ/\mathrm{d}$$

$$(n_{\mathrm{S}} = 0.986^\circ/\mathrm{d},\ n_{\mathrm{M}} = 13.246^\circ/\mathrm{d})$$

$$\alpha\dot{\omega} + \beta\dot{\Omega} + \gamma n_{\mathrm{Moon}} \approx 0$$

(lunar semi-secular res)

Phase-space cartography

Solar semi-secular resonances

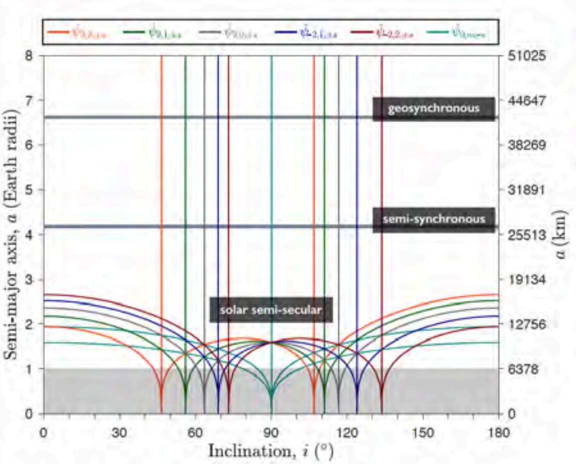

The oblateness *apsidal* and *nodal* precession overshadows the lunisolar effects

$\dot{\omega} \approx 4.98 (R/a)^{\frac{7}{2}} \frac{5\cos^2 I - 1}{(1-e^2)^2}$ °/d

$\dot{\Omega} \approx -9.97 (R/a)^{\frac{7}{2}} \frac{\cos I}{(1-e^2)^2}$ °/d

$\dot{\Omega}_M \approx -0.053°/\mathrm{d}$

$(n_S = 0.986°/\mathrm{d}, n_M = 13.246°/\mathrm{d})$

$$\alpha\dot{\omega} + \beta\dot{\Omega} + \gamma n_{\mathrm{Sun}} \approx 0$$

(solar semi-secular res)

Phase-space cartography

Lunar secular resonances

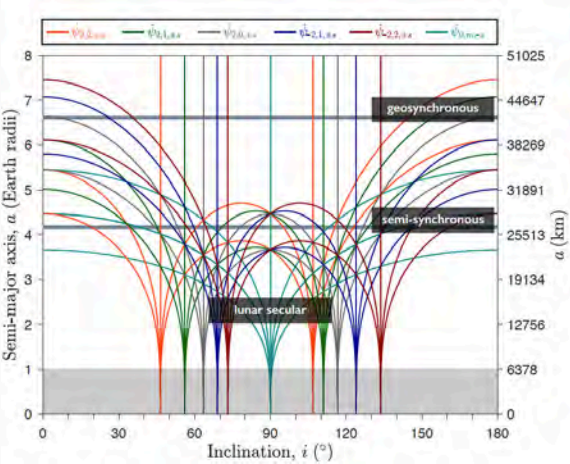

The oblateness *apsidal* and *nodal* precession overshadows the lunisolar effects

$$\dot{\omega} \approx 4.98(R/a)^{\frac{7}{2}} \frac{5\cos^2 I - 1)}{(1-e^2)^2}\,{}^\circ/\mathrm{d}$$

$$\dot{\Omega} \approx -9.97(R/a)^{\frac{7}{2}} \frac{\cos I}{(1-e^2)^2}\,{}^\circ/\mathrm{d}$$

$$\dot{\Omega}_{\mathrm{M}} \approx -0.053^\circ/\mathrm{d}$$

$$(n_{\mathrm{S}} = 0.986^\circ/\mathrm{d}, n_{\mathrm{M}} = 13.246^\circ/\mathrm{d})$$

$$\alpha\dot{\omega} + \beta\dot{\Omega} + \gamma\dot{\Omega}_{\mathrm{Moon}} \approx 0$$

(lunar secular res)

Phase-space cartography

Combined resonance web

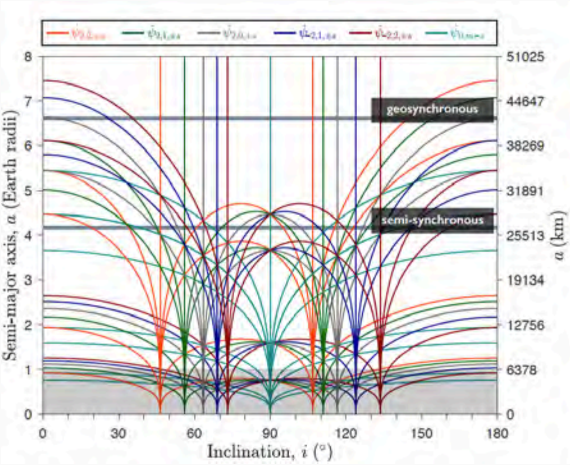

The oblateness *apsidal* and *nodal* precession overshadows the lunisolar effects

$\dot{\omega} \approx 4.98(R/a)^{\frac{7}{2}}\frac{5\cos^2 I - 1}{(1-e^2)^2}$ °/d

$\dot{\Omega} \approx -9.97(R/a)^{\frac{7}{2}}\frac{\cos I}{(1-e^2)^2}$ °/d

$\dot{\Omega}_{\mathrm{M}} \approx -0.053°$/d

($n_{\mathrm{S}} = 0.986°$/d, $n_{\mathrm{M}} = 13.246°$/d)

$\alpha\dot{\omega} + \beta\dot{\Omega} + \gamma n_{\mathrm{Moon}} \approx 0$

(lunar semi-secular res)

$\alpha\dot{\omega} + \beta\dot{\Omega} + \gamma n_{\mathrm{Sun}} \approx 0$

(solar semi-secular res)

$\alpha\dot{\omega} + \beta\dot{\Omega} + \gamma\dot{\Omega}_{\mathrm{Moon}} \approx 0$

(lunar secular res)

Phase-space cartography

Analytical studies are then complemented by *numerical cartographies* of the phase space.

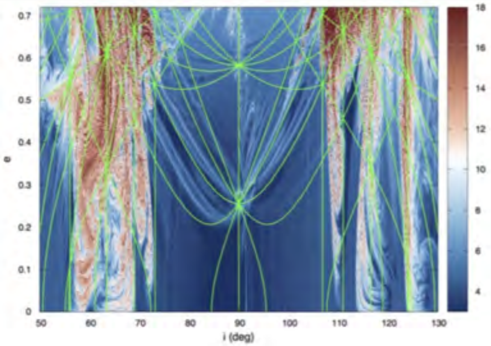

Daquin, Gkolias, and Rosengren (2018)

Chaos indicators, or *their proxies*, are employed to measure stability.

Phase-space cartography

Background information

Goals of the study

Phase-space cartography

- Overview of methods
- Implementation
- Results

Estimation of collision probability

- Background theory
- Implementation
- Results

Summary of key findings

Conclusions

THALASSA orbit propagation code

THALASSA is a Fortran orbit propagation code integrating *non-averaged* equations of motion (LSODAR subroutine).

The user can choose between several sets of *regularized* (i.e., non-singular) equations of motion.

Formulation	Variables	Time el.	Reference
Cowell	Coord.	None	several, see Montenbruck & Gill (2000)
Kustaanheimo-Stiefel (KS)	Coord.	Lin.	Stiefel & Scheifele (1971)
Stiefel-Scheifele (SS)	Elem.	Lin.	Stiefel & Scheifele (1971)
EDromo	Elem.	Const., lin.	Baù et al. (2015)

Numerical cartography of OneWeb MEO

Definition of the region of initial conditions for the OneWeb MEO constellation:

	Nominal	Interval
t_i	Jan 1 2020, 00:00:00 TT	—
h	8500 km	$\pm$200 km
e	0	—
i	45°	$\pm$3°
Ω	0°	360°
$\omega + M$	0°	—

	Nominal	Interval
t_i	Jan 1 2020, 00:00:00 TT	—
h	7500 km	$\pm$200 km
e	0	—
i	45°	$\pm$3°
Ω	0°	360°
$\omega + M$	0°	—

Simulation duration: 93.0 years (5 lunar nodal periods)

Physical model:

- 5×5 geopotential
- drag (NRLMSISE-00)
- lunisolar perturbations from analytical ephemerides
- SRP with conical shadow
- $A/m = 0.01\,\mathrm{m^2\,kg^{-1}}$ ($0.15\,\mathrm{m^2\,kg^{-1}}$ with sail), $C_D = 2.2$, $C_R = 1.2$.

Numerical cartography of OneWeb LEO

Definition of the region of initial conditions for the OneWeb LEO constellation:

	Nominal	Interval
t_i	Jan 1 2020, 00:00:00 TT	—
h	1200 km	$\pm$200 km
e	0	—
i	87.9°	$\pm$2°
Ω	0°	360°
$\omega + M$	0°	—

Simulation duration: 93.0 years (5 lunar nodal periods)

Physical model:

- 5×5 geopotential
- drag (NRLMSISE-00)
- lunisolar perturbations from analytical ephemerides
- SRP with conical shadow
- $A/m = 0.01\ \mathrm{m^2\,kg^{-1}}$, $C_D = 2.2$, $C_R = 1.2$.

Phase-space cartography

- **Background information**
- **Goals of the study**
- **Phase-space cartography**
  - Overview of methods
  - Implementation
  - Results
- **Estimation of collision probability**
  - Background theory
  - Implementation
  - Results
- **Summary of key findings**
- **Conclusions**

OneWeb MEO phase space views

Maximum eccentricity e_{max} is a reliable, although somewhat flawed, indicator of orbital stability.

Numerical map for $a_0 = 13\,870$ km

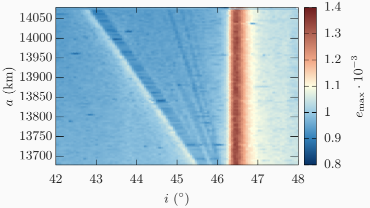

Numerical map for $a_0 = 13\,870$ km with solar sail

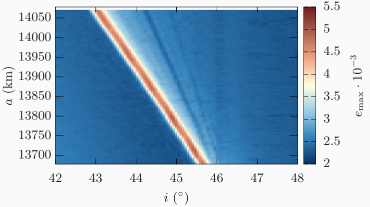

Numerical map for $a_0 = 14\,870$ km

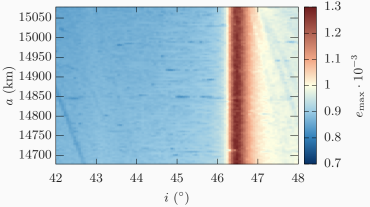

Analytical map for $a = 13\,675$ km - $14\,075$ km

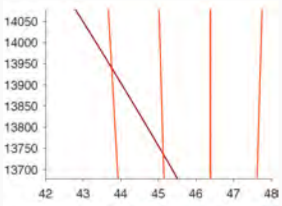

OneWeb LEO phase space views

Results are as expected based on analytical resonance map.

OneWeb LEO *is* stable.

Numerical map for $a_0 = 7578$ km

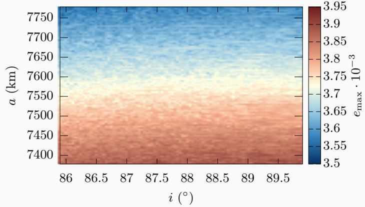

Analytical map for $a = 7378$ km - 7778 km

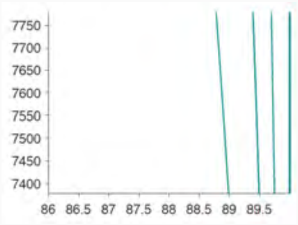

Estimation of collision probability

Modified Öpik and Wetherill approach

Objects are assumed to be moving on independent Keplerian orbits about a central body.

Öpik (1951) derived an equation for when one of the objects is moving in a circular orbit.

Wetherill (1967) generalized the solution for two eccentric orbits.

JeongAhn and Malhotra (2017) simplified the derivation.

Modified Öpik and Wetherill approach

The theory begins with the calculation of the collision probability for two intersecting Keplerian orbits.

$$P(\tau, \vec{\alpha}_1, \vec{\alpha}_2) \tag{1}$$

The objects are fixed in space and mean anomalies are asssumed independent.

Over a long period of time the objects will have a well defined collision probability at their intersection.

Modified Öpik and Wetherill approach

The collision probability with respect to an ensemble of field bodies can also be determined.

(a, e, i) are assumed to be fixed and (Ω, ω, τ) are assumed to be random stochastic variables.

Recent studies have been performed where the secular evolution of (Ω, ω, τ) is adopted in order to integrate P.

- Rickeman et al. (2014)
- JeongAhn and Malhotra (2015))

Modified Öpik and Wetherill approach

The velocity is assumed to be linear near the point of intersection.

$$\rho(\vec{t}) = \vec{r} + t\vec{v} \qquad (2)$$

At the point of intersection we equate $\rho(\vec{t})$ of each object.

$$\vec{r}_1 + t_1\vec{v}_1 = \vec{r}_2 + t_2\vec{v}_2 \qquad (3)$$

Linearized velocities of two object near intersection point

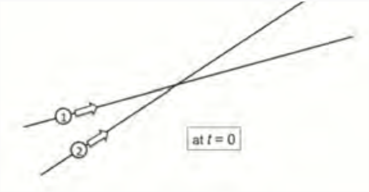

Credit: JeongAhn and Malhotra (2017)

Modified Öpik and Wetherill approach

The relative encounter velocity is given by:

$$\vec{U} = \vec{v}_1 - \vec{v}_2 \qquad (4)$$

Taking the cross product of each side with $\vec{(U)}$ yields:

$$(\vec{r}_1 - \vec{r}_2) \times \vec{U} = (t_1 - t_2)(\vec{v}_1 \times \vec{v}_2) \qquad (5)$$

Linearized velocities of two object near intersection point

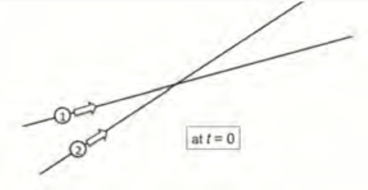

Credit: JeongAhn and Malhotra (2017)

Modified Öpik and Weaherill approach

Suppose the minimum value of $|\rho(\vec{t})_1 - \rho(\vec{t})_2|$ occurs at some time t:

$$D_{min} = |\vec{r}_1 + t\vec{v}_1 - \vec{r}_2 + t\vec{v}_2| \quad (6)$$

Setting $t = 0$:

$$D_{min} = |\vec{r}_1 - \vec{r}_2| \quad (7)$$

Modified Öpik and Wetherill approach

THE UNIVERSITY OF ARIZONA

At the minimum distance, the encounter velocity vector $\vec{U}$ is normal to $(\vec{r}_1 - \vec{r}_2)$.

Taking the absolute values of both sides of equation 5 :

$$|(\vec{r}_1 - \vec{r}_2) \times \vec{U}| = (t_1 - t_2)|(\vec{v}_1 \times \vec{v}_2)| \tag{8}$$

Rearranging:

$$(t_1 - t_2) = \frac{|\vec{r}_1 - \vec{r}_2||\vec{U}|}{|(\vec{v}_1 \times \vec{v}_2)|} \tag{9}$$

$$\Delta t = \frac{D_{min}|\vec{U}|}{|(\vec{v}_1 \times \vec{v}_2)|} \tag{10}$$

Modified Öpik and Wetherill approach

A collision can only occur if at the time $t = t_1$, body two is within Δt_{col} of the intersection point.

Positions at times $t = t_1$ and $t = t_2$

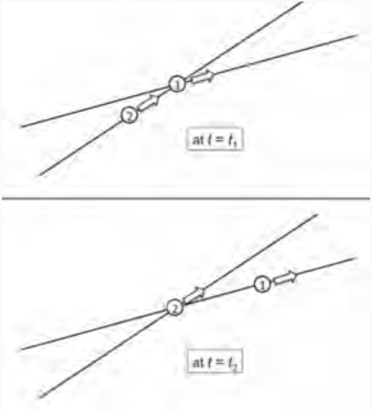

Credit: JeongAhn and Malhotra (2017)

Modified Öpik and Wetherill approach

THE UNIVERSITY OF ARIZONA

Because body one passes the intersection point once per period, the probability that body two is within Δt_{col} at the same time is given by:

$$P_1 = \frac{2\Delta t_{col}}{T_2} \tag{11}$$

Probability per unit time is found by deviding by T_1.

$$P_= \frac{2\Delta t_{col}}{T_2 T_2} \tag{12}$$

Modified Öpik and Wetherill approach

For non-intersecting orbits, collision is still possible if $s < \tau$.

If body two is shifted by by $\vec{s} = (0, 0, -s)$:

$$\vec{r}_1 + t_1\vec{v}_1 = \vec{r}_2 - \vec{s} + t_2\vec{v}_2 \quad (13)$$

Letting D_{min} occur once again at $t = 0$:

$$D_{min} = |\rho(\vec{0})_1 - (\rho(\vec{0})_2 - \vec{s})|$$
$$D_{min} = |\vec{r}_1 - \vec{r}_2 + \vec{s}| \quad (14)$$

Positions at times $t = t_1$ and $t = t_2$

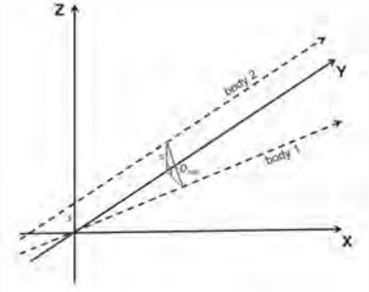

Credit: JeongAhn and Malhotra (2017)

Modified Öpik and Wetherill approach

THE UNIVERSITY OF ARIZONA

From the figure observe that:

$$|\vec{r}_1 - \vec{r}_2 + \vec{s}| = \sqrt{{D_{min}}^2 - s^2} \tag{15}$$

Positions at times $t = t_1$ and $t = t_2$

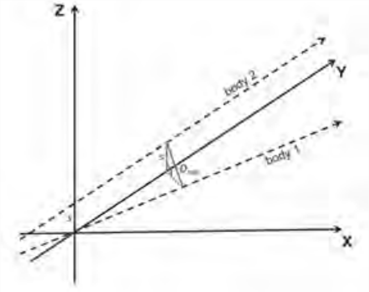

Credit: JeongAhn and Malhotra (2017)

Modified Öpik and Wetherill approach

THE UNIVERSITY OF ARIZONA

Because $\vec{U}$ is normal to both $\vec{s}$ and $(\vec{r}_1 - \vec{r}_2)$:

$$\begin{aligned} |(\vec{r}_1 - \vec{r}_2 + \vec{s}) \times \vec{U}| &= |(t_1 - t_2)(\vec{v}_1 - \vec{v}_2)| \\ |(\vec{r}_1 - \vec{r}_2 + \vec{s})||\vec{U}| &= (t_1 - t_2)|(\vec{v}_1 - \vec{v}_2)| \end{aligned} \tag{16}$$

Therefore, when $D_{min} = \tau$ and $\tau < s$:

$$\Delta t_{col} = \frac{\sqrt{1 - \frac{s^2}{\tau^2}} U}{|\vec{v}_1 \times \vec{v}_2|} \tag{17}$$

Modified Öpik and Wetherill approach

THE UNIVERSITY OF ARIZONA

Averaging over s in the range 0 to τ and inserting into equation 12 yields:

$$P_{avg} = \frac{\pi \tau U}{2|\vec{v}_1 \times \vec{v}_2| T_1 T_2} \tag{18}$$

Estimation of collision probability

Simulation Methods

Applying the Öpik-Wetherhill approach to the initial planes of the satellites fails to capture the dynamics of the problem.

Our solution is to create a distribution of clones by propagating the satellite trajectories over some period of time.

For an arbitrary target satellite in each orbital plane, the individual *averaged* probabilities of the clones satisfying $s < \tau$ are summed to yield:

$$P_{plane} = \frac{N_p}{N_c} \sum P_i(\vec{\alpha}_1, \vec{\alpha}_2) \quad (19)$$

Simulation Methods

When the number of clones satisfying $s < \tau$ is sparse, an inflation factor, I, can be applied and then corrected for.

$$P_{plane} = \frac{1}{I^2}\frac{N_p}{N_c}\sum P_i(\vec{\alpha}_1, \vec{\alpha}_2) \tag{20}$$

The accuracy of the results is evaluated through a comparison to close approaches generated by a brute force numerical simulation of constellation satellites.

Estimation of collision probability

Preliminary Results

Considering the evolution of field objects over the course of one year.

N_c	time span	I	τ	$\sum P$	time of next collision
365	365 days	10	$2m$	$3.774E-08\frac{1}{s}$	306 days

Preliminary Results

Considering the evolution of field objects over the course of 10 days and comparing with a numerical simulation of constellation satellites.

N_c	time span	I	τ	$\sum P$	time of next collision
365	10 days	0	$50m$	$2.214E-05\frac{1}{s}$	0.523 days

Preliminary Results

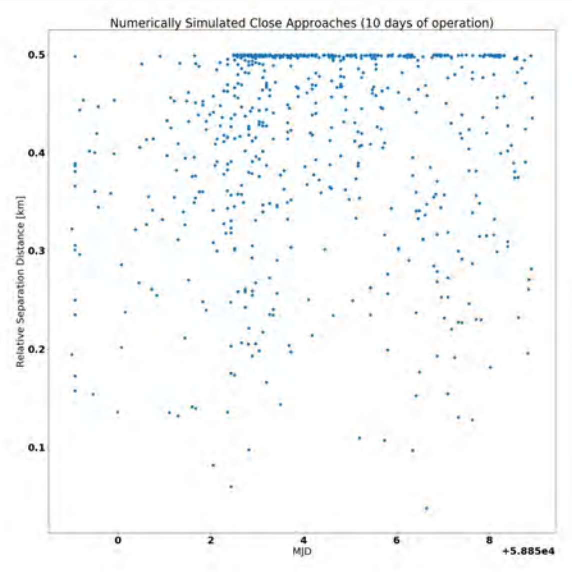

Key Findings

The regions of near-Earth space around the OneWeb MEO and LEO constellations are stable.

At 7500 km, the amplitude of the SRP resonance can be slightly increased with the deployment of a modest-sized solar sail.

Our probalistic study predicts an endogenous collision of OneWeb LEO satellites after 306 days

Conclusions

THE UNIVERSITY OF ARIZONA

Phase-space cartography:

There are resonances in the same region of space as the proposed OneWeb constellations that cause small changes to eccentricity.

These resonances are not drastic enough to be used for disposal. In MEO a graveyard scheme is recommended.

In LEO a drag disposal scheme is recommended.

Longer timescales for re-entry might allow us to use these resonances.

Conclusions

THE UNIVERSITY OF ARIZONA

Collision probability estimation:

The comparison to numerically simulated trajectories indicates room for improvement.

In the future different methods of generating clones as well as different multiplicities of clones should be investigated.

Explore the efficacy of minimum space occupancy constellations. Early results are very promising.

Explore collision risk during re-entry.